Proceedings of the 7th International Symposium on Cavitation
CAV2009 – Paper No. 136
August 17-22, 2009, Ann Arbor, Michigan, USA

Air Entrainment Mechanisms from Artificial Supercavities: Insight based on numerical simulations

Michael P. Kinzel **Jules W. Lindau** **Robert F. Kunz**
Penn State University
Applied Research Laboratory
State College, PA, USA

ABSTRACT

Using multiphase computational simulations based on the Navier-Stokes equations, we examine the internal gaseous flows of artificially ventilated supercavities. These simulations indicate that air shear layers that develop on the cavity-wall (the air-liquid interface surrounding the cavity) are an important mechanism of air entrainment. This corroborates previous theory developed for toroidal cavities, and indicates that similar mechanisms occur in twin-vortex cavities and cavities closing on bodies. The importance of these shear layers on the cavity behavior potentially impacts computational simulations, experiments, and design-level models. Lastly, a more inclusive, semi-empirical air entrainment model is presented that attempts to accommodate the observed processes.

INTRODUCTION

Concept high-speed underwater vehicles surrounded by a ventilated gaseous supercavity (supercavitating vehicles) are potentially advantageous compared to fully wetted vehicles of similar mission. The primary benefit of supercavitation is drag reduction, which is thought to enable very high-speed vehicles. The benefit of ventilation versus vaporous cavitation is cavity stability. Stable cavities of course are also important. Buffeting, surface damage, large-scale vehicle vibrations and other negative consequences typically result from vaporous cavitation. With an artificially inflated cavity, the absence of a condensing gas alleviates this effect. Unfortunately, with such a vehicle, a supply or source of air must be carried onboard, introducing the gas economy problem. The gas economy problem presents the question of how much air must be carried to satisfy a given supercavitating vehicle mission. In this paper, an assessment of models and dynamics of the cavity air, which directly affects the amount of air to be carried, is performed.

In a supercavitating vehicle, the hull form is typically designed for the cavitating flow conditions. This is analogous to supersonic aircraft, and their designs are specific to supersonic flight. Thus, the hull-form should be designed to be enclosed by a gaseous supercavity at supercavitation conditions of interest. Adequately enclosing the vehicle within the supercavity minimizes the viscous-drag and prevents cavity destabilization. Furthermore, design of vehicle subcomponents, propulsion, lifting surfaces, etc. require a predictive understanding of the precise supercavity shape. Geometric restrictions create the need for design-level models to approximate the cavity location, and an understanding of the controlling parameters that affect it.

Supercavitating vehicle operation depends on an ability to supply air sufficient to fill the cavity. This problem may be reduced to ascertaining the amount of air entrained by the cavity, for given cavity conditions, size, vehicle speed, etc. Obviously this is equivalent to knowing the needed air supply rate to sustain a steady cavity and directly corresponds to air storage requirements. A characteristic feature of the supercavity is the cavity-closure type Typically they are classified as either twin- or toroidal-vortex cavities. Cavity-closure mode influences cavity stability and also appears related to the dominant mechanisms of air entrainment.

In this work, computational fluid dynamics (CFD) is used to investigate the physical processes of air entrainment. Such a method, if successful, can provide the information needed for analysis and visualization without difficulties associated with physical observation of supercavities. Of course, in any framework other than direct numerical simulation, it is necessary that CFD-discovered phenomena must be validated experimentally.

Using CFD solutions, we deduce mechanisms of air entrainment. In particular, evidence appears that corroborates theory, presented by Spurk [1], tying air-entrainment to cavity-wall shear layers. The original work by Spurk [1] was limited to toroidal-vortex closing cavities. Although not surprising, the reviewed CFD solutions display evidence that the cavity-shear layers are also a primary mechanism of the air-entrainment from twin-vortex-closing cavities. Using such observations, an improved form of modeling the air-entrainment rate is proposed. Finally, this mechanism may not conform with the conventional viewpoint on supercavity air entrainment.

BACKGROUND

Theory developed for modeling supercavities, cavity-closure modes, and the impact these closure modes have on the physical mechanisms of air entrainment is reviewed. The viewpoint and all investigations are restricted to horizontal supercavities driven behind an axisymmetric cavitator. Therefore buoyancy is considered and acts perpendicular to the free stream velocity. It is also known that the quality of the cavity interface may have a strong effect on the amount of air entrained. In this effort we restrict our consideration to cavities that separate rather cleanly from a cavitator and interfaces that, over the majority of the cavity length, appear laminar or nearly

so. The various air-entrainment rate mechanisms lead to models dependent on the cavity closure mode.

Theoretical Cavity Predictions

Scaling parameters and selected semi-empirical methods used to model supercavities are reviewed. From these semi-empirical methods a closure problem arises introducing the need to model the air-entrainment rate

Useful Scaling Parameters

Several nondimensional quantities are typically considered for the scaling of ventilated supercavities. The primary factor is the cavitation number, σ_c, and is defined as

$$\sigma_c = 2\frac{p_\infty - p}{\rho_\infty V_\infty^2}. \qquad (1)$$

This is a nondimensional cavity pressure. It also inversely relates to cavity size (as cavity pressure increases so does cavity size). The air ventilation rate, Q, is normally nondimensionalized by the cavitator diameter, D_N, and free-stream speed, V_∞.

$$C_Q = \frac{Q}{V_\infty D_N^2} \qquad (2)$$

It is useful within these parameterizations to use an *equivalent disk-cavitator diameter*, rather than the actual cavitator diameter thereby replacing D_N with $D_{N,Disk}$. The definition of $D_{N,Disk}$ is given in Eq. 3.

$$D_{N,Disk} = D_N\sqrt{\frac{c_D}{c_{D,Disk}}} \approx D_N\sqrt{\frac{c_D}{0.82(1+\sigma)}}. \qquad (3)$$

The flat circular disk cavitator of a size that yields the same drag as a given cavitator under consideration would be referred to $D_{N,Disk}$. This is convenient as, cavity size and shape should scale with cavitator drag. Most conveniently, when generated by an axisymmetric cavitator at zero angle of attack, the drag then equivalences the cavities made by cavitators of differing geometric shapes. Thus, C_Q can be defined using the equivalent disk diameter (as in Eq. 3) and the cavity size and shape should correspond to the cavity created behind another cavitator of the same drag. Note that the relation for $C_{D,Disk}$ substituted in Eq. 3 is a linear form based on experimental behavior presented in May [2]. Lastly, the Froude number, Fr_N, is a strong scaling parameter given by

$$Fr_N = \frac{V_\infty}{\sqrt{gD_N}}, \qquad (4)$$

where g is the gravitational constant. Again, basing Fr_N on the disk, or $Fr_{N,Disk}$, is a common and useful convention.

Other independent scaling parameters are less significant. For example, the Reynolds number, $Re_N=\rho_\infty V_\infty D_N \mu_\infty^{-1}$, is not important for scaling supercavities [3]. Also, typical supercavity applications involve high free stream velocities and large cavities with mostly small curvature. Therefore, the Weber number is large, and effects from surface tension should be negligible.

Cavity Shape Approximations

Potential flow assumptions are common for handling the stable regions of supercavities. Analytic solutions, based on elliptical cavities at the limiting case of $\sigma_c=0$, combined with empiricism enable quick, reliable, and accurate methods to predict twin-vortex cavity shapes as presented by Semenenko [3] and Logvinovich [4]. These methods use integral parameters such as drag coefficients, c_D, cavitator radius, R_N, and σ to define the cavity shape. This includes the cavity radius, R_c (defined in Eq. 5), the cavity length, L_c (defined in Eq. 6), and the axial profile, $R(x)$ (defined in Eq. 7). Here, R_c is defined as

$$R_c = R_{N,Disk}\sqrt{\frac{c_{D,Disk}}{k\sigma}}, \qquad (5)$$

where k is an empirical parameter that is about 1.0. An approximation of L_c is given as

$$L_c = 2R_{N,Disk}A\frac{\sqrt{c_{D,Disk}}}{\sigma}.$$

The empirical parameter A is around 2.0. Finally, for a disk-cavitator, the cavity radius can be expressed along the cavity length as

$$R(x)=\begin{cases} R_N\left(1+3x/R_N\right)^{1/3} & for: x \le x_1 \\ R_c\sqrt{1-\left(1-\frac{R_1^2}{R_c^2}\right)\left[1-2\left(x-x_1\right)\left(L_c-2x_1\right)^{-1}\right]^{2/\kappa}} & for: x > x_1 \end{cases}. \qquad (7)$$

In this relation, another empirical parameter, κ, is introduced, which is also approximately unity. Also, x_1 is the location where the two relations are matched; these relations define the region where the cavity separates from the cavitator geometry for $x \le x_1$, and the analytic cavity shape for $x > x_1$. A matching length, x_1, of $2R_N$ is typically used. The one-third relation, for $x \le x_1$, is well suited for disk-shaped cavitators, but can be easily substituted for another relation that can represent other cavitator shapes.

Finally, one can also consider buoyant cavities. Based on the momentum theorem, the axis deflection of the supercavity is a result of the combined effects of cavity buoyancy and downwash from a lifting cavitator. This is directly computed, as given in Semenenko [3], as

$$h(x)=\left[\frac{g}{\pi V_\infty}\int_0^x \frac{Q(s)}{R(s)^2}ds\right]_{bouyancy} - \left[\frac{c_L D_N^2}{8}\int_0^x \frac{1}{R(s)^2}ds\right]_{Lift}. \qquad (8)$$

Here, $R(x)$ is the local cavity radius and $Q(x)$ is the volume of cavity air occupied from x=0 to x. The separate gravity and lift

terms are indicated with subscripts and c_L is the cavitator-lift coefficient.

The above relations provide an efficient, and accurate, prediction of the cavity shape. The cavity shape along the axis (Eq. 7) can simply displaced using the effect of gravity and lift (Eq. 8). In general, the only unknown quantities are the forces on the cavitator, i.e. c_L, c_D. The remaining parameters are either specified (i.e. V_∞, ρ_∞, σ_c) or empirical (i.e. k, κ, and A). Closure of these relations require approximations or models of the air-entrainment rate for a given cavity pressure, σ_c. For steady ventilation rates, the cavity size can then be determined. This process motivates and exploits the Fr-dependent C_Q-σ_c relations of air entrainment and the motivation for improving such models.

Cavity-Closure Modes

Prior to discussing the models of air entrainment, it is important to understand cavity-closure modes and their impact on air entrainment rate. In this work, only two closure modes are examined; these being the previously mentioned twin-vortex and toroidal-vortex cavity-closure patterns. Diagrams of the cavity types are displayed in Fig. **1**. These types of closure modes are generally descriptive of cavities generated by axisymmetric cavitators in a mean flow perpendicular to the gravity force vector and closing without obstruction. Cavities closing with interference from a body or pierced by control surfaces may still be approximated by the following discussion, but there are additional complications.

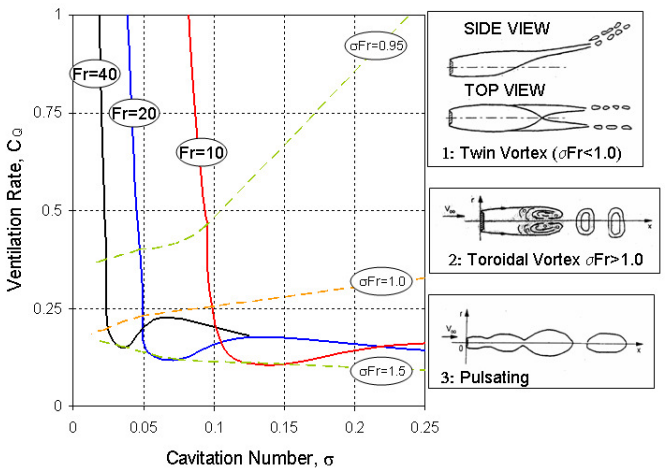

Figure 1: Sample C_Q-σ curve with corresponding cavity types. The diagrams are from Semenenko [3].

Twin-vortex closing cavities are rather large, stable, cavities that are obviously formed under the influence of a buoyant force. As these cavities are longer than toroidal closure cavities, they are more subject to buoyant effects. It was empirically determined by Campbell and Hilborne [5] that twin-vortex cavities form when $\sigma Fr_{N,Disk}$ values are less than unity. The salient feature of such cavities is the axially aligned, twin-vortex structure that forms at the cavity closure. These twin vortices contain the entrained cavity air.

With negligible or little relative gravitational effects, the toroidal-vortex cavity form occurs. Empirical evidence [5] suggests that these cavities form for $\sigma Fr_{N,Disk}$ values of greater than unity. At the cavity terminus, axisymmetric reentrant jets form into toroidal-shaped vortices that shed from the cavity. These vortices contain the entrained cavity air.

Air-Entrainment Models

As previously discussed, steady supercavitation requires the air to be supplied at the same rate it is leaked. As a result, it is easier to close the problem inversely, that is by establishing the air-entrainment rate for a given cavity size. The idea here is to develop models for C_Q over a range of cavity sizes. And then using this modeled behavior to determine σ, or the cavity size, at a given C_Q. These models are discussed for both cavity-closure types.

Twin-Vortex Cavities

The major mechanism of air-entrainment from a twin-vortex-type cavity is through the vortex tubes. Multiple models of air entrainment exist. Campbell and Hilborne [5] presented a model of air entrainment based on a correlation of the circulation about the cavity centerline, to the buoyant loads on the cavity. This circulation correlates to the radius of the twin vortex cores, which results in the first expression of Eq. 9. Note that V_{VT} is the velocity of the air traveling out of the cavity, through the core of the vortex tube. Using approximations of the R_C and L_C, similar to Eqs. 5 and 6, and assuming that V_{VT} is roughly V_∞, Eq. 9 is becomes a fully closed expression for the air entrainment as approximates in the last relation.

$$C_{Q,CH} = \frac{\pi}{32 Fr_{N,Disk}^4 \sigma}\left(\frac{V_{VT}}{V_\infty}\right)\left(\frac{D_C}{D_{N,Disk}}\frac{L_C}{D_{N,Disk}}\right)^2 \approx \frac{\pi}{15.8 Fr_{N,Disk}^4 \sigma^4} \tag{9}$$

Note that differences between experiments and theory are expected to be a direct result of errors in the assumed value of V_{VT} [5]. Thus, we introduce the entrainment model in a form where V_{VT} may be modified via an improved model, and to maintain consistency with Eqs. 5 and 6 for $D_C/D_{N,Disk}$ and $L_C/D_{N,Disk}$. A slightly modified form is presented as

$$C_{Q,CHm} \approx \frac{\pi A^2 (1+\sigma)^2}{47.6 k Fr_{N,Disk}^4 \sigma^4}\left(\frac{V_{VT}}{V_\infty}\right). \tag{10}$$

Note that a disk-drag behavior of $c_{D,Disk} \approx 0.82(1+\sigma)$ is assumed, and recall that the parameters A and k are empirical parameters that are roughly 2.0 and 1.0, respectively.

Toroidal-Vortex Cavities

The air entrainment from cavities with toroidal-vortex closure occurs via gaseous, toroidal-shaped, shedding cavities. Recent theory from Spurk [1] suggests that mechanisms occurring upstream of these toroidal vortices are important, and that the air transported along interfacial shear layers to the end of the cavity consists of the air that eventually fills the toroidal cavities. The general concept is displayed in the diagram presented in Fig. **2**, where the concept of the air-cavity shear layers entraining air from the cavity is displayed. Here, a shear

layer forming within the air forms at the air-water interface; the air in this shear layer remains attached to the water and becomes the air that eventually escapes from the cavity.

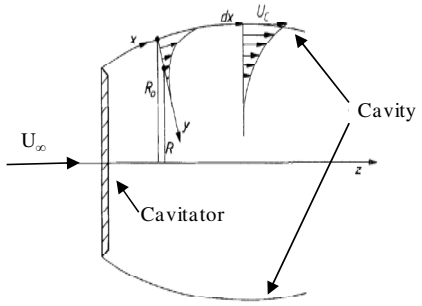

Figure 2: Diagram of the air-boundary layers within a cavity, theorized as an important mechanism for air entrainment. The diagram is from Spurk [1].

This concept of cavity-shear layers dragging air from the cavity was previously hypothesized, as mentioned in May [2], however, was only recently incorporated into a valid air entrainment model by Spurk [1]. The theory agrees well with experimental measurements at high Fr_N conditions and for reentrant cavities with little buoyant effects. In a reduced, rather general, form, Spurk's air-entrainment model is given as

$$C_{Q,Spurk} = k_Q \frac{(1+\sigma)}{\sigma}\sqrt{\frac{1}{\sigma}\ln\frac{1}{\sigma}}, \qquad (11)$$

where k_Q is an empirically determined constant that is based on a single reentrant cavity data point. Note that other forms of this entrainment model based on laminar or turbulent boundary layers are presented, however, this empirical form is used as it calibrates well for both laminar and turbulent shear layers.

DESCRIPTION OF COMPUTATIONAL METHODS

Computations are performed using the finite-volume solver, UNCLE-M, which is described by Lindau *et al.* [6]. The solver is valid for n-species and is valid for homogenous-mixture multiphase simulations. The codes incorporates higher-order numerics, RANS/DES/MILES turbulence modeling approaches, and the use of structured-overset grids. Furthermore, the solution technique is applicable for incompressible, mixture-energy-conserving compressible flows, and flows with liquid-vapor phase change. Spatial and temporal requirements have already been determined to be sufficient by Kinzel [7].

In these simulations, the interface of a cavity is explicitly defined from the transport of the species mass. Thus, the gaseous and liquid regions are fully described by the Navier-Stokes equations. The realizable-scaled level-set method described in Kinzel [7] is also used to alleviate dissipating the interface. Wall functions based on Spalding's boundary layer model are applied. The approach is reasonable from the viscous sublayer to the log-region of the boundary layer. Such an approach is extremely useful for the multiphase flows of interest, where with the mixed air or water regions, the needed wall spacing can vary considerably.

Some general assumptions are present in the numerical simulations. First, most cases model the attached liquid boundary layers as laminar. This is justified by considering the -favorable pressure gradients that characterize flow on the cavitators. All flows are treated as incompressible; this has potential to affect instantaneous pressure fields but is expected have a minor impact on the largely stable cavities examined. Finally, homogenous multiphase assumptions are invoked, i.e., it is assumed that no slip velocities exist between the air and water. This is valid for these cases based on the following arguments: (1) buoyant-driven velocities and time scales are small relative to the convective length of the supercavity; (2) velocity gradients are low in the mixture regions, implying that equilibrium in velocities of each constituent is to be expected; finally, (3) we are fully resolving the primary bubble of interest.

COMPUTATIONAL RESULTS

Using CFD simulations of multiphase supercavitating-fluid flows, that resolve much of the dynamics of the liquid, air, and viscous regions of the flow field, the mechanisms of air entrainment can be examined. Such an application of CFD is useful, as visualization of numerical simulations is straightforward. Experimental-based visualization, on the contrary, encounters visualization difficulties within the gaseous regions. For example, smoke visualization has a tendency to fill the cavity and not yield much insight. Particle image velocimetry (PIV), suffers from light and laser sheet distortion and light refraction that makes it impossible to visualize through foamy cavities. Thus visualization issues are eliminated with a Navier-Stokes-based CFD approach. In addition the viscous effects on the dynamics of the air filled cavity can be systematically investigated.

Description of Test Cases

Several representative test cases are used in these analyses. The cases include isolated cavitators and cavities interacting with bodies.

Axisymmetric Disk Cavitator

A ventilated disk cavitator is represents a basic case. Two conditions are simulated for this geometry: (1) a limiting case at $Fr_N=\infty$, $Re_N=90\times10^6$, $C_Q=0.5$; and (2) a case based on the experiments of Campbell and Hilborne [5] $Fr_N=15.54$, $Re_N=62{,}200$, at a range of C_Q values. For the buoyant cases, solution is three-dimensional with assumed lateral symmetry. Additional details are described in Kinzel [7].

Cone-Shaped Cavitator

A 15°-half-angle, conical cavitator based on a summary of experiments by Kiceniuk [8], is also investigated. The cavitator is set to a lifting configuration, relevant for trimming or maneuvering a vehicle. Based on the actual diameter, rather than the commonly used effective-disk diameter, the corresponding conditions are: $Re_N=3.2\times10^7$, $Fr_N=72.0$, and $C_Q=1.0$. Additional details of the modeled geometry, mesh, resolution studies, and validation are available in Kinzel [7].

Supercavitating Body

Lastly, a case with significant cavity-body interactions is investigated. The case is based on experiments conducted in the University of Minnesota, St. Anthony Falls Laboratory's high-speed water tunnel [9][10]. Conditions corresponding to Re_N of 56,000, Fr_N=26.7, and a range of C_Q values were simulated. Results compared favorably with the experiments. However, the favorable outcome was dependent on modeling of a support strut, requiring fully three-dimensional integration with no assumed symmetry, as reported in the work of Kinzel *et al.* [11]. These experiments and simulations display a Gilbarg-Efros-type closure, where the cavity terminates with a reentrant jet onto the body [9]. The geometry of the body is modeled as specified by Schauer [10]. However in the present effort, since it does not impact the physics under consideration the aforementioned support strut is omitted. Additional details can be found in the work of Kinzel [7].

Air Entrainment Behavior

Consider the method of air-entrainment proposed by Spurk [1], this suggests that shear layers should be the evident mechanism in determining the amount of entrained air. A local rate of air entrainment is defined, and given as

$$C_{Q,l} = \alpha_g \, u / V_\infty \, . \tag{12}$$

This variable highlights aftward moving air through the cavity, which can be (roughly) interpreted as entrained air.

Cavity Air Escaping a Twin-Vortex Cavity

To the authors' knowledge, previous theories of air leakage from twin-vortex cavities neglected shear-layer regions as mechanisms of air entrainment. However, based on these CFD simulations, it becomes clear that it is fundamental component of the entrained air. This process is first investigated on the twin-vortex supercavity forming behind cone-shaped cavitator, and is presented in Fig. **3**. In these plots, a grey-scale contour plot along the centerline highlights the cavity in black. Several contour-line plots at various axial locations display the $C_{Q,l}$ contour levels, and streamlines of the cavity flow are pictured. In Fig. **3**, the values of $C_{Q,l}$ are clearly highest near the cavity interface. This strongly suggests that gaseous axial flow occurs due to water tugging on air, a clearly expected physical process. However, this process continues through to the vortex tubes and dominates the air entrained from the cavity.

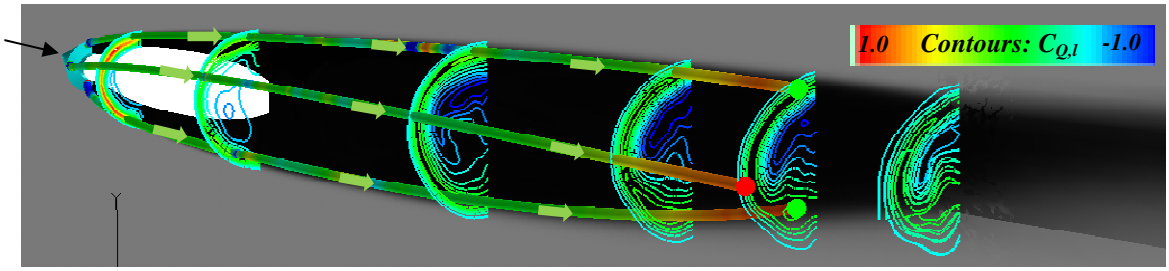

(a) Streamlines traced backwards from the maximum $C_{Q,l}$ regions

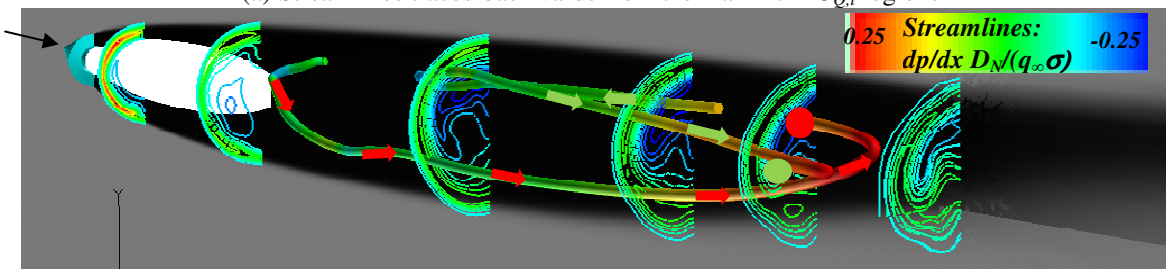

(b) Streamlines traced backwards from the minimum $C_{Q,l}$ regions

Figure 3: Air entrainment and recovery for twin vortex cavity on a cone cavitator. The cavitator is colored cyan and the oncoming velocity is indicated by the black arrow. The streamlines (colored by pressure gradient) are traced backwards to indicate the origin. The contour lines display the local air entrainment rate, $C_{Q,l}$. The background is a contour plot of the air volume fraction with black indicating air.

Streamlines indicating the flow history are also displayed in Fig. **3**. These streamlines are traced backward in time from various $C_{Q,l}$ magnitudes at the penultimate $C_{Q,l}$ contour plot. It is presumed that, at this aft axial station, positive $C_{Q,l}$ values indicate entrained air that will exit the cavity. In Fig. **3** (a), the streamlines are traced from the maximum $C_{Q,l}$ level. These streamlines all originate from the injection port, suggesting that the injected air is immediately entrained into the shear layer and proceeds directly out of the cavity. To examine the history of recirculating air, in Fig. **3** (b), the streamlines are traced originating from the most negative $C_{Q,l}$ values. The air in the core of this cavity then behaves like a wake. There is some interaction with the interface shear layer, but the net forward flow in the wake region is zero. This picture suggests that some air from the core becomes entrained by the interface shear layer along the length of the cavity, but is stripped from the shear layer near the cavity terminus. Although Spurk's hypothesized flow structure, characterized by the interface attached shear-layer [1], is clearly observed in this twin-vortex cavity, additional physical processes are apparent. Namely, that these shear layers can be thinned as they approach the cavity terminus.

Air Escaping a Reentrant Cavity Formed Over a Body

Air entrainment from a cavity surrounding, and impinging on, a vehicle body is examined. Streamlines are used to investigate the predicted airflow through the supercavity and shown in Fig. **4**. The red streamlines are seeded aft of the vehicle, in the air that is clearly entrained from the cavity, and are traced backward. As before, the streamlines indicate a clear path from the ventilation ports, into the shear layers, and out of the cavity region. The purple streamlines are seeded within the cavity region; here the cavity air remains isolated and recirculates within the cavity.

Also in Fig. **4**, a contour plot of $C_{Q,l}$ is provided along the plane of symmetry. The predicted cavity interface is pictured with the grey isosurface, clipped just outside the centerline to allow visualization within the cavity. Consider the air flow away from the shear layer entrainment region. It is evident that $C_{Q,l}$ is only positive near the ventilation ports, and quickly diminishes away from these ports as the air recirculates back towards the cavitator, and is finally entrained along the cavity interface. Along the interface, high positive values of $C_{Q,l}$ are observed, indicating that the air is pulled to the rear of the cavity through shear-layer mechanisms. The flow hypothesized by Spurk [1] is again observed for modeled cavities interacting with a body.

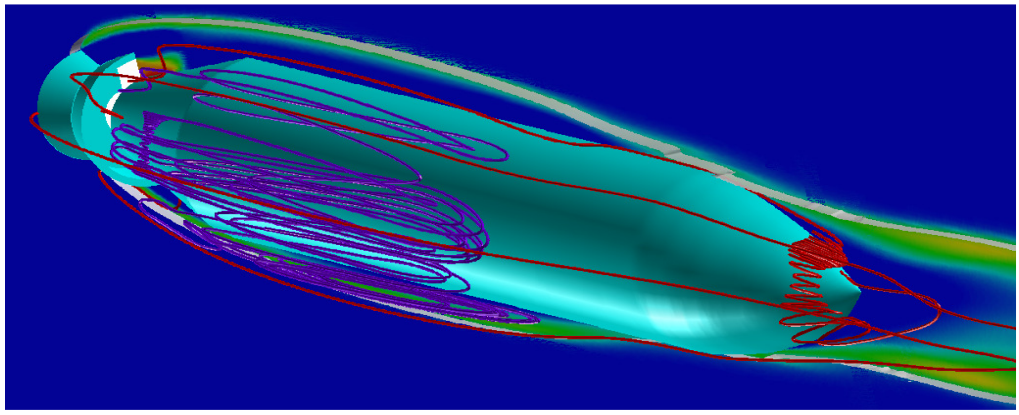

Figure 4: RANS prediction of a ventilated supercavitating body at C_Q=0.45, Fr_N=26.7, Re_N=56,000. The contours display the local air entrainment, $C_{Q,,l}$, and the streamlines indicate the path of the entrained air (red) versus cavity air (purple).

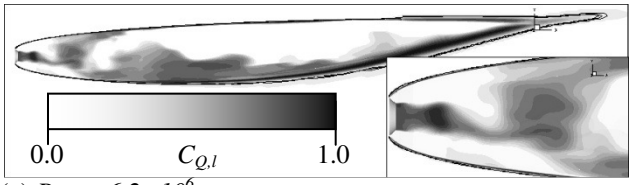

(a) $Re_N = 6.2\times10^6$

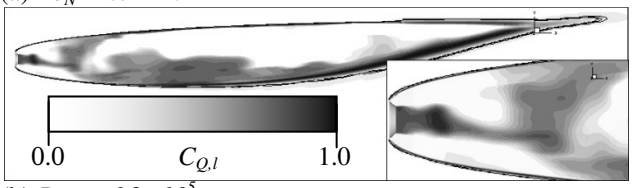

(b) $Re_N = 6.2\times10^5$

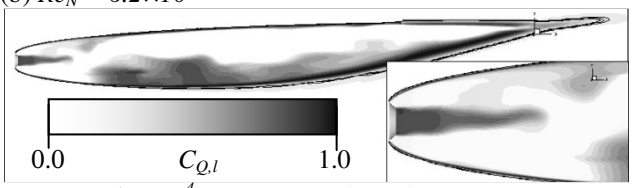

(c) $Re_N = 6.2\times10^4$ *(Experimental conditions)*

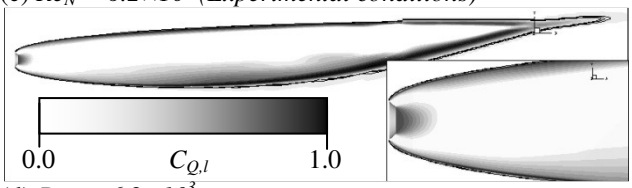

(d) $Re_N = 6.2\times10^3$

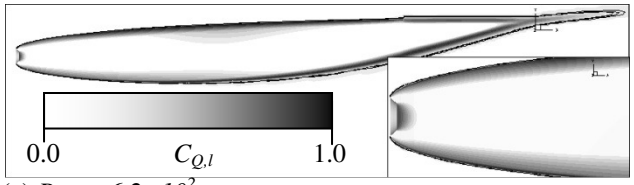

(e) $Re_N = 6.2\times10^2$

Figure 5: Reynolds number effect on the supercavitating flow occurring around a disk cavitator at C_Q=0.283 and Fr_N=15.54. The filled contour plot through the centerline displays $C_{Q,l}$. The black contour lines outline the location of the cavity interface. Note that the air is ventilated on the back face of the cavitator.

Reynolds Number Effects in a Twin-Vortex Cavity

Reviewed modeling tends to suggest the importance of cavity shear layers as a mechanism of air entrainment. Consequently, one would expect *Re* effects evident in the shear layer regions. Such studies highlight the effects expected with a lack of *Re* scaling. In Fig. **5**, contour plots of $C_{Q,l}$ are displayed at varied Re_N values. In this model, the ventilation port covers about 2/3 of the rear face of the cavitator. The air jet exiting the port appears to be highly sensitive to the Re_N value. At increased Re_N values (6.2×10^4 to 6.2×10^6) the jet extends axially, then eventually dissipates roughly two cavitators diameters downstream of the jet. Following the dissipation of the jet, the air appears to be entrained into the shear layer. Alternatively, for low Re_N values (6.2×10^2 to 6.2×10^3), the jet immediately dissipates and the cavity shear layers thicken just downstream of the separation point from the cavitator. In this

vicinity, the shear layer thickness displays a strong Re_N effect. In Fig. **5**, one can easily see the trend of increased shear-layer thickness with a decreasing Re_N. Interestingly, following the dissipation of the jet, the cavity-shear-layer thickness does not display a strong Re_N effect.

DISSCUSSION

The development of these air-shear layers and their impact on the air entrainment rate is crucial for many analysis methods. In this section, we highlight potential issues resulting from these shear layers.

CFD Predictions: Influence of Shear Layer Importance

The accurate prediction of the C_Q-σ_c relation for a supercavitating-fluid can be sensitive to the approach that these gaseous shear layers are handled. This is, of course, dependent on the solution method. For example, potential flow methods eliminate this effect as the cavity air is modeled (rather than simulated). Therefore, in these approaches the amount of entrained air most come from another correlation. However, in viscous simulations where the fluid dynamics of each phase is considered, the treatment of these shear layers should be important (Kinzel *et al.* [12]). Here we briefly discuss how the modeling approach effects the results of the simulations.

It is customary, to interpret the effect of turbulence on mean flow via an effective or eddy viscosity. However, models of the eddy viscosity rely on empiricism that tunes it to a specific turbulent region, which is most often for the turbulent wall-bounded flows. Using such an approach, modeling issues arise in other turbulent shear layer regions, i.e. the viscous sublayer within the boundary layer and separated flows. In single-phase flows, the wall bounded viscous sublayer is accommodated using damping functions to moderate the turbulence model near the walls and large scale separated flow may be simulated (rather than modeled) using approaches such as Detached-Eddy Simulation (DES). This ultimately yields a physically reasonable model of turbulence. According to Spurk's theory [1] and the present computational results, complexities of single-phase flows exist with the addition of shear layers that also appear to be air boundary layers on the air-water interface. In terms of cavity predictions, the modeled turbulence levels at the cavity interface are intimately connected to the modeled air shear layer and ultimately the simulated air entrainment rate and/or the C_Q-σ_c relation.

Examination of the Turbulence Model Effects

Turbulence model sensitivities are evaluated for the axisymmetric disk cavitator configuration. The most straightforward and extreme comparison is an evaluation of a particular case with and without RANS-type turbulence modeling (RANS vs. no TM). This comparison is made on a single computational grid. A high-resolution mesh through the interface regions is used in these studies, specifically, $\Delta r \sim 0.01 R_N$ corresponding to roughly sixty cells through the cavity-interface shear layers. The predicted air-shear layer velocity profiles near the cavity interface are displayed in Fig. 6 enabling comparisons with and without turbulence modeled. The intention is to understand the limits, or bounds, of the possible solutions. In this plot, a measure of velocity magnitude on the horizontal axis, and the vertical axis is the inward distance from the cavity interface. A velocity of one indicates that the air is traveling at the same speed of the water, positive velocities indicate forward , and negative velocities indicate reversed flow.

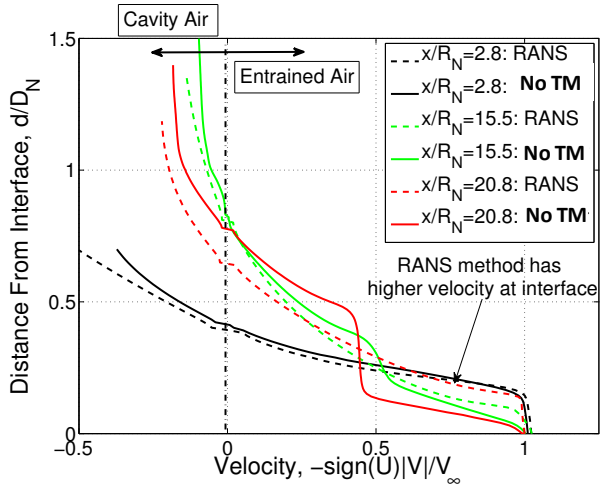

Figure 6: Predicted cavity boundary layers for the axisymmetric disk cavitator using RANS and simulation with no turbulence model (no TM). The plotted distance is from the cavity interface, radially into the gaseous cavity. The velocity magnitude is chosen to allow for the effects of skewness of the cavity and the sign(U) distinguishes entrained air from recirculating air in the cavity.

The general trend indicates significant differences between results obtained from the two modeling approaches. Just past the cavitator, by 2.8 disk radii, there is little difference between the solutions with and without turbulence models, indicating minimal localized influence of modeled turbulence. However, progressing further aft of the cavitator, 15.5 and 20.8 radii, the solutions progressively deviate. This deviation indicates differences arising from an integrated effect; consistent with the boundary layer hypothesis. As the deviations are examined, the laminar profiles exhibit a more rapid decrease from the water velocity at the interface, than does the RANS case. The RANS case, having a greater quantity of air moving close to liquid velocity, i.e. exhibiting a larger displacement thickness, entrains more air. It is clear that there is direct link with the turbulence modeling approach and the amount of air within this layer.

On further inspection, considering the results with no TM, the solutions tend to approach a roughly constant velocity region just outside of the shear layer. This is consistent with the conservation of mass for the axisymmetric, steady flow. Thus, the area integrated air velocity profile must be equal between the two cases. As the laminar case displays thinner shear layers, a consistent C_Q is achieved through the increased centerline velocity to compensates for the net decrease in the shear layer.

This computational investigation suggests that the amount of air entrained into the cavity-shear layers can be impacted by the turbulence modeling approach. Considering RANS relative to no TM, the amount of shear-layer entrained air is increased.

This is expected to be a result of the modeled eddy viscosity thickening, i.e. increasing the entrainment mechanisms of, the shear layer.

Specific Issues with Turbulence Model Behavior

It is apparent from the preceding case that the approach to modeling turbulence impacts air entrainment in the cavity shear layers. By review of fully three-dimensional, unsteady supercavitating flow simulations, additional insight into the turbulence model behavior may be deduced. In this case, the cavity is forced to close on a body. The predicted eddy viscosity field, ν_t, for a Detached Eddy Simulation (DES) and an Unsteady RANS (URANS) simulation at similar cavitation, Reynolds, and Froude numbers are shown in Fig. **7**. Note the peak in the modeled eddy viscosity at the interface; however, the DES simulation clearly exhibits lower values in eddy viscosity than the URANS. As is expected of a turbulent simulation method intended to resolve features in wake-like separated flows, it appears that the general formulation of DES reduces this effect. In comparison to the values near solid surfaces, where the turbulence model damping functions reduce the eddy viscosity, the values are too high in the cavity interface shear layers, which is not desired. However, it was shown, by Kinzel *et al*. [12], that the capture of the correct C_Q-σ_c relation was sensitive to the turbulence modeling approach, and that the DES formulation captures the trend well. When the DES modeling approach has been applied, even in cases where the resolution and time-step sizes are expected to be too coarse for proper turbulent simulation, the results are improved fortuitously. This improvement appears due to the reduction in modeled eddy viscosity away from physical walls. These evident turbulence modeling deficiencies may be overcome via a modified approach, appropriately treating interface attached shear layers.

(a) URANS

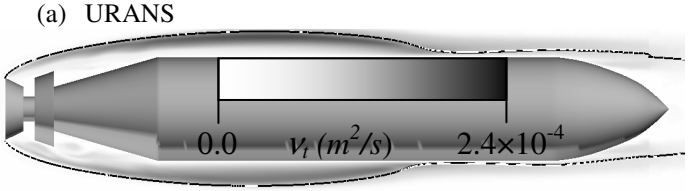

(b) DES

Figure 7: Comparison of the predicted cavity (α=0.5 contour displayed with a black line) and the modeled eddy viscosity using URANS and DES turbulence model.

Impact of Shear Layers on Experiments

Despite the expected presence of interface attached shear layers, in assessment of supercavitating objects, Re_N scaling is not normally considered a factor. Thus far, the shear layer assessments presented have focused on effects that are limited in scope due to the idealization of the case. Practical configurations are not limited to isolated cavitators. If Re_N scaling does, in fact, alter the air-entrainment rate, the effect seen on an isolated cavitator is expected to be less pronounced than in more complex, i.e. practical, configurations. Other factors dependent on Re_N scaling manifested in the gaseous cavity flow may also exist. In particular, CFD predictions presented in Kinzel *et al.* [12] suggested that geometric-induced hysteresis effects are sensitive to the eddy viscosity. Additional practical considerations such as interface stability and interaction with ventilation schemes are also expected to be Reynolds number dependent and must be considered for scaling of real applications.

IMPROVED MODELS OF AIR ENTRAINMENT

It is suggested that the theory of Spurk [1], previously validated for slender, reentrant, axisymmetric supercavities, is applicable to buoyant ones as well. This hypothesis is based on insight gained through supercavity computations. The current level of numerical modeling may not capture all of the relevant physics, principally the interfacial air shear layer is not adequately modeled. High interface-perpendicular resolution reduces the magnitude of this issue, along with other observed deficiencies, such as the turbulence model sensitivities. This type of error reduction via increased resolution is consistent with the overall shear layer based entrainment conjecture. Based on this behavior, we modify current air-entrainment models to account for the observed effects. These effects include (1) shear layer contributions to the air entrained from a twin-vortex cavity and (2) stripping of volume from this displacement layer by mechanisms at the rear of the cavity. It is noted that due to streamline convergence in the external liquid flow, a pressure increase will always be expected at the rear of twin vortex cavities. This elevated pressure should have a thinning effect on the attached shear layers, diminishing the volume flow of entrained air that actually leaves the cavity. The air returning to the cavity will be considered *recovered,* while the remaining entrained air rides in a diminished shear layer as it enters the vortex tubes. Because the interface-attached, air boundary layer profile is actually thinned, steepened, and *stabilized* through this adverse pressure gradient, it is by no means undergoing the same process as a classic boundary layer separation. Therefore, although tempting, we avoid the word *separation*.

Concept Overview

Incorporating the observed physical mechanisms into air entrainment models should improve such models. Combining previously developed models, i.e. the approach of Spurk [1] based upon cavity-shear layers for toroidal closure cavities and of Campbell and Hilborne [5] for twin-vortex cavity closure, a more complete model is possible. Incorporation of the observed mechanisms of entrained shear-layer thinning at the cavity closure is also needed.

In Fig. **8**, components of the model are presented. The shear layers, or more precisely estimations of an effective displacement thickness, are colored grey. The regions outside of the shear layers, colored white, is the cavity-flow region, which is assumed to recirculate within the cavity. This is

conceptually analogous to hydrodynamic design approaches that model external flows as inviscid and use integral boundary-layer methods to obtain a displaced surface and shear surface forces. Of course, the true cavity air is anything but inviscid flow as it is mostly a recirculatory wake. However, restricting this to a lumped-volume perspective, inviscid assumptions are sufficient.

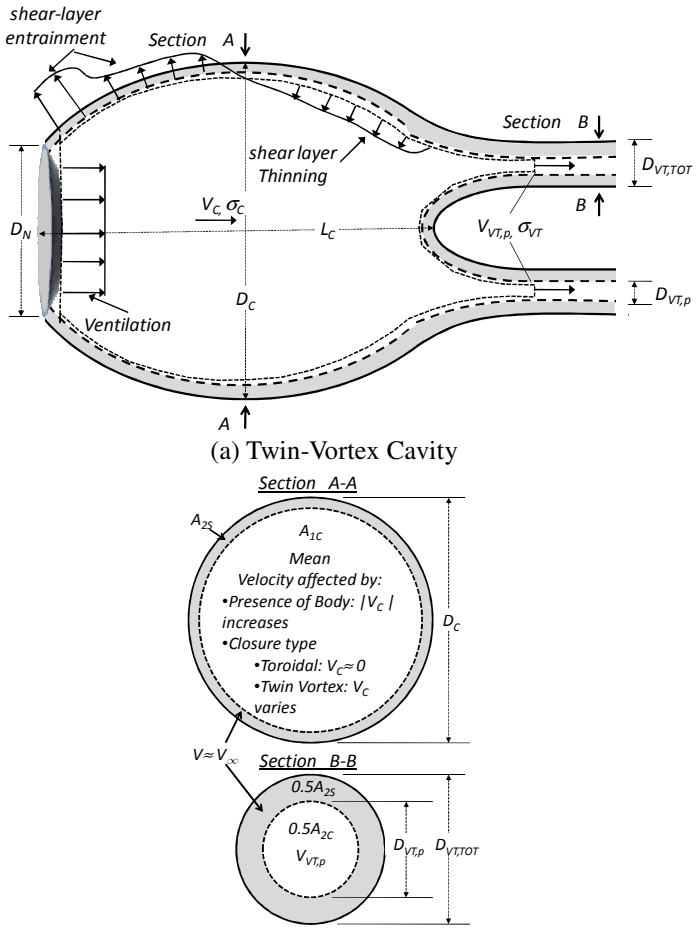

(a) Twin-Vortex Cavity

(b) Sectional properties

Figure 8: Elements of economy in a twin-vortex cavity. The gray regions of the cavity represent the air within the interfacial shear layers. The white regions represent the *cavity* regions, not directly impacted by the water flow.
(a) Near-horizontal plane through the cavity containing cavitator, cavity, and both vortex tubes.
(b) Two selected axial planes. A-A through the maximum cavity radius location. B-B is through one of the vortex tubes.

Some initial points can be made about the modeling approach conceptualized in Fig. **8**. Based on agreement with the theory of Spurk [1], toroidal cavities tend to have a net zero axial flow within the white *cavity* region. Essentially, the gray regions directly fill the shedding toroidal cavities. With twin-vortex closure, complexities in this concept arise. Thus, several points are mentioned before going through the model, as outlined below:

(1) *Cavity-Shear Layer Velocity:* The shaded-gray regions of the cavity are assumed to travel at the velocity of the neighboring water flow, i.e. $V_{SL} = V_\infty \sqrt{1+\sigma}$, however, for simplicity, V_{SL} is assumed to be equal to V_∞ at entry to the vortex tubes.

(2) The case of $V_c < 0$ and $V_{TV,p} = 0$, for $C_Q < C_{Q,SL}$: The condition occurs when the vortex tubes are too small to allow the assumed entrained shear-layer air to freely exit the cavity (at the free stream velocity). Assuming that the vortex tube radius is governed by the circulation of water flow around the cavity [5] and that the cavity shear-layer air velocity is that of the neighboring water flow, this condition occurs. Note that based on the assumed modeling, the amount of entrained shear-layer air brought to the rear portion of the cavity is independent of closure behavior. Thus, in the condition where the vortex tubes are too small to allow 100% of the cavity-interface entrained air to flow through the assumed vortex tubes at less than or equal to the free stream velocity, a portion of the shear layer entrained air must be stripped from the shear region and reenter the cavity.

(3) The limiting case of $V_c = 0$ and $V_{TV,p} = 0$, for $C_Q = C_{Q,SL}$: In this case, the assumed vortex tubes have sufficient cross sectional area to relieve the air within the shear layers, i.e. the ventilation rate Q is equivalent to $2V_\infty A_{VT,TOT}$. Note that shear layer thinning at the aft and of the cavity will cease to be significant.

(4) The case of very high ventilation rate, $V_c > 0$ for $C_Q > C_{Q,SL}$: The vortex tubes open to an area larger than the shear layer air can provide, promoting pressure-gradient driven axial flow through the tubes. In this case, the amount of shear layer entrained air is actually enhanced by the wake flow.

(5) *When a body is present*: If the body is fully contained within the white-cavity region, thus *does not interfere with the cavity-shear layer*, these entrainment mechanisms remain (at least under point (2)) nearly unaffected. Although, the magnitude of the axial velocities within the cavity may be increased due to area constrictions, this has little effect on the eventual flow through the vortex tubes. This is consistent with conventional thinking that solid objects internal to an established cavity should not affect the cavity ventilation requirements or shape.

These considerations shape the proposed model. In general, we propose a model composed of multiple components, given by

$$C_Q = C_{Q,SL} + C_{Q,p} \,. \tag{13}$$

Here, $C_{Q,SL}$ is the contribution from shear-layer effects, paralleling Spurk [1]. $C_{Q,p}$ is driven by pressure gradients, and is derived from the work of Campbell and Hilborne [5].

Shear-Layer Air Entrainment

The entrained-air-through-shear-layers mechanisms is first modeled. Although the method presented by Spurk [1] fully accounts for the air entrained in the shear layers, it does not consider the quantity that might be stripped off the shear layer at cavity closure by an adverse pressure gradient. This concept is essentially an addition to the model of Spurk.

Recovery Factor

The quantity stripped from the shear-layer, or recovered air, can be determined by considering the remaining mechanisms effecting air entrainment. Here we quantify recovered air by taking the difference between the ventilation rate and the volume flow rate in the theoretical cavity interface shear layers. The flow rate in the shear layers is obtained using Eq. 11, and calibrated to a toroidal cavity for a given Fr_N and Re_N. To study this effect, consider a recovery factor defined as

$$C_Q = \left(1 - k_{RQ}\right) C_{Q,Spurk} \rightarrow k_{RQ} = 1 - \frac{C_Q}{C_{Q,Spurk}}. \qquad (14)$$

Physically, k_{RQ} is the fraction of air initially entrained by the cavity-shear layer that is recovered and returned to the cavity. Estimating values of k_{RQ} given the air-entrainment rate should yield an improved modeling of air entrainment. Note that Eq. 14 only remains valid for $C_Q < C_{Q,SL}$. Regardless, it is easy to ascertain the validity of this approach based the so-obtained reasonable k_{RQ} values, discussed below.

Positive k_{RQ} values represent air recovery (from the liquid attached shear layer). When k_{RQ} is between zero and one, a portion of the cavity-shear layer air is recovered and returned to the cavity. Without accounting for this air recovery, a straightforward application of Spurk [1] over predicts the air entrainment rate. Note that, via alteration of the undisturbed cavity air flow, it seems possible that other forms of recovery could occur.

This air recovery is the observed mechanism in the CFD simulations and, since it represents a decrease in the air displacement thickness is thought of as a thinning of the liquid-attached shear layer. Note that since the rear of the cavity is smaller in diameter than the center, as the entrained air is drawn aftward, the local displacement thickness may not necessarily be getting smaller. However, the integrated *displacement area*, at least, must get smaller. Also, since the natural consequence of this process is a more stable boundary layer, even though recovered air is forced back into the wake due to an adverse pressure gradient, it is not referred to as a boundary layer separation.

Negative k_{RQ} values indicate that the total ventilation rate is higher than that entrained by the boundary layers, implying that an additional mechanism of entrainment is occurring and cavity shear layers may become less significant. Presumably, in this condition, a favorable axial pressure gradient exists. This is contrary to the weak adverse gradient expected for the case of a positive k_{RQ}. Small to moderate negative values of k_{RQ} may be within the range of observed cavity behavior. However, very large negative values of k_{RQ} imply excessive ventilation and are probably not desirable.

Recovery Factor Behavior in Hysteretic Cavities

The data collected in experiments conducted by Campbell and Hilborne [5], include hysteretic phenomena with twin-vortex and toroidal cavity closures. It is noted here that cavity hysteresis has been demonstrated to occur over a range of ventilation rates for horizontal, buoyant cavities aft of axisymmetric cavitators. (See, e.g. Campbell and Hilborne [5] for a more complete discussion of the hysteresis.) This data is useful to further develop the general physics of air-entrainment and the recovery factor. The particular data set applied here was developed from measurements using a ventilated circular disk cavitator running at $Fr_N=16$ and $Re_N=62{,}000$. In Fig. **9** (a), a straightforward application of Eq. 11 (the unmodified model developed by Spurk [1] for non-buoyant cavities) is compared to the data. The Spurk theory yields an excellent prediction for the toroidal cavities occurring on the right portion of the curve, through the increasing-C_Q hysteresis region. Beyond the hysteresis region, Eq. 11 clearly over predicts the ventilation rate (C_Q) required for a given cavity pressure (σ_c). In the present modeling effort, the amount over predicted by Eq. 11 is assumed to be recovered air. Assessed in terms of k_{RQ}, and computed using Eq. 14, these quantities are plotted in Fig. **9** (b).

The trends in Fig. **9** (b), the k_{RQ}-σ_c plot, are as expected with some particularly interesting behavior in the hysteretic (gray shaded) region. For toroidal cavities, k_{RQ} remains near zero. For twin-vortex cavities, k_{RQ} is bound between zero and one, suggesting that cavity shear layer recovery is occurring. Lastly, an interesting feature is observed. For the twin-vortex regime (Q-decreasing curve), k_{RQ} is maximized at a near constant value of 0.64. This behavior implies that, in this region, the relative amount of air recovered from the entrainment shear layer remains constant and that the separated shear layer could be a dominating contributing mechanism to hysteresis. For the toroidal-vortex cavity, on the Q-increasing curve, k_{RQ} takes on a small negative value just prior to the cavity transition to twin-vortex. Perhaps, this is due to toroidal structures entraining additional cavity wake air along with the shear layer entrained air. Regardless, the consistency of the modeling with the data supports the concept of k_{RQ}.

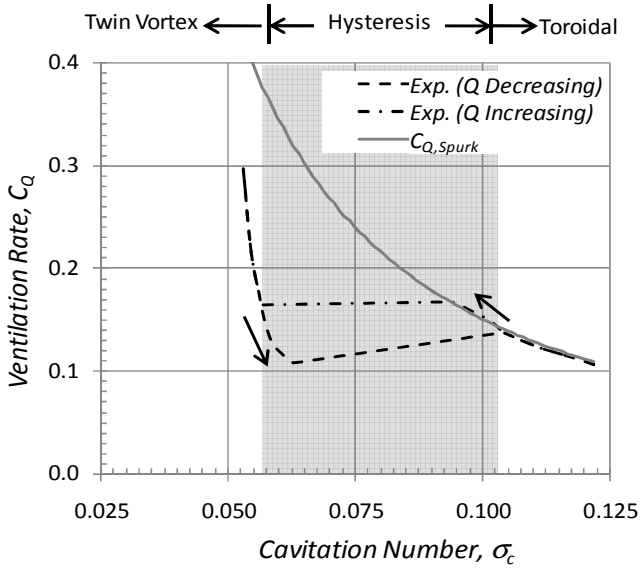

(a) C_Q-σ_c curves

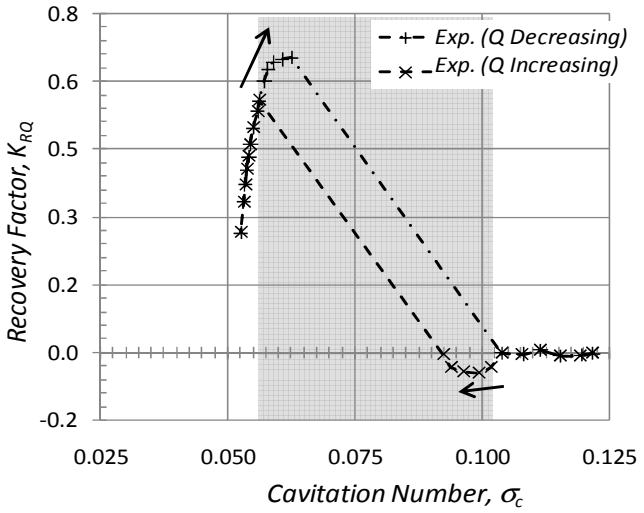

(b) Corresponding k_{RQ}, behavior

Figure 9: In part (a), is a comparison of a hysteretic C_Q-σ_c curve for a disk cavitator, from Campbell and Hilborne [5], to theory of Spurk [1]. Part (b) displays the corresponding k_{RQ} curves, for the hysteretic cavity is provided.

Approximating the Recovery Factor

Using physical arguments and experimental data, the recovery factor can be approximated. On the C_Q-σ_c space, there are essentially three regions that need to be considered, i.e. twin-vortex, hysteretic, and toroidal. Using Cambell and Hilborne's data [5], a path to approximate this behavior is proposed. First, we assess k_{RQ} as a function of σFr; this incorporates, the empirically determined, twin-vortex to toroidal transition criterion. Thus, a Heaviside function enforces this criterion in the k_{RQ} approximation for σFr values greater than one [5], i.e. $H(1-\sigma Fr)$. For the twin-vortex range, outside of the hysteresis region, a polynomial function with a minimum at $\sigma Fr = 1$, $k_{RQ}=1$ is fit to the. Finally, it was observed above that within the hysteretic region of the twin-vortex cavities k_{RQ} is maintained at a constant value, $k_{RQ,Hys}$. This and a minimal value of zero are used to bound the function. The approximation is given as

$$k_{RQ}(\sigma Fr) = \max\left(\min\left(A_0 + A_2(\sigma Fr - 1)^2, k_{RQ,Hys}\right), 0\right) H(1-\sigma Fr), \quad (15)$$

where the values of A_0 and A_2 were determined via a least squares fit to the data. For this specific, Campbell and Hilborne [5], case, A_0=0.815, A_2=-17.36, $k_{RQ,Hys}$=0.654, and the Heaviside function is approximated as $H(1-\sigma Fr) \approx 0.5[1+\tanh(1000\{1-\sigma Fr\})]$. The results of this are plotted below in Fig. **10**. Note that the approximation follows the data quite well.

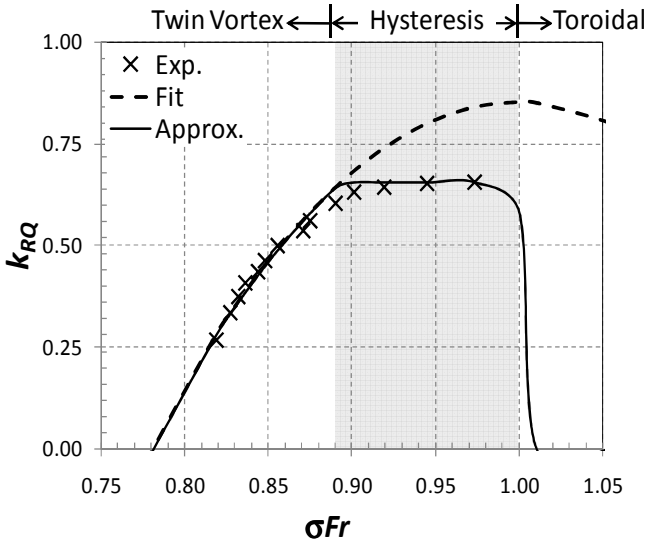

Figure 10: Recovery factor versus σFr for the experiment and approximate function. Note that the fit is a polynomial fit to the data left of the hysteresis region.

The modeling appears to conform well to this particular case. The amount of shear layer entrained air, $C_{Q,SL}$, from Eq. 14 using the empirical correction to the recovery factor, k_{RQ}, is compared to experimental measurements in Fig. 11. It is apparent that the model performs well throughout the experimental data. However, it appears that, approaching the highest C_Q and lowest σ_c values, the model behaves aphysically.

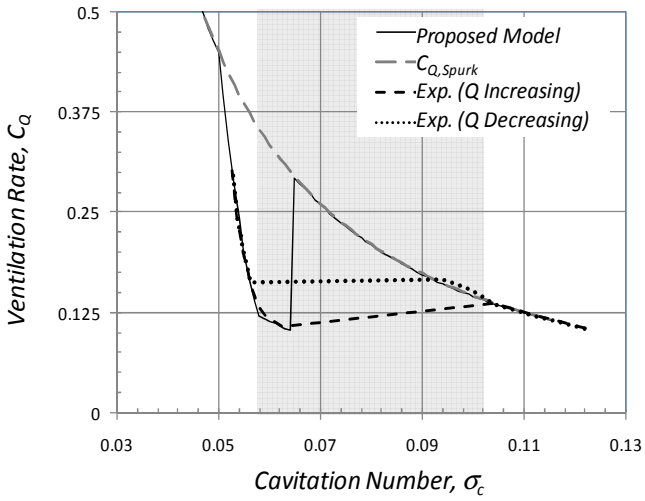

Figure 11: Predicted air entrainment rates using the proposed model with shear recovery, Spurk's model ($C_{Q,Spurk}$), and experiments from Campbell and Hilborne [5].

Although the presented approximation is a fit to data, a model is preferred. Such a model could enable an analytic function that remains valid over a range of conditions. It is presumed that this approximation is valid only for this particular Re_N and Fr_N. However, with additional data the parameters A_0, A_2, and $k_{RQ,Hys}$ could be empirically determined

using extended Re_N and Fr_N data sets and optimization algorithms, and should enable the approximation to be valid over various cavitator configurations and conditions.

Shear-Layer Air and Hysteresis

Consider the model behavior with respect to experimental measurements displayed in Fig. 12. $C_{Q,CHm}$, (Eq. 10) with an assumed vortex velocity, $V_{VT}=V_\infty$ is compared to $C_{Q,Spurk}$ (Eq. 11) and hysteretic experimental data [5]. Interestingly, $C_{Q,CHm}$ and $C_{Q,Spurk}$ intersect within the twin-vortex cavity hysteresis region.

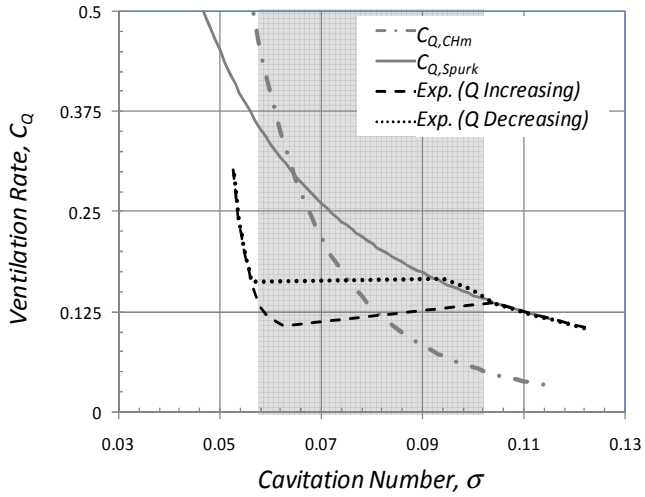

Figure 12: Predicted air entrainment rates using Campbell & Hilborne's model ($C_{Q,CHm}$), Spurk's model ($C_{Q,Spurk}$), and experiments from Campbell and Hilborne [5].

The point of intersection of the $C_{Q,CHm}$ and $C_{Q,Spurk}$ curves appears to be related to the phenomenon. Based on the presently developed physical models, this intersection occurs when the twin vortex tubes are sufficiently large to support the shear-layer air with no recovery. As this value of σ_c roughly corresponds to the smallest, decreasing-C_Q, twin-vortex cavity reported from the experiments, it may be an indicator of the mechanism that induces the transition from twin-vortex back to toroidal cavity closure. Perhaps, it may be interpreted that the cavity remains in a twin-vortex state provided that the vortex tubes can support the entrained air within the cavity attached shear layers.

However, this differs from the previous suggestion that, rather than fully being transported out the vortex cores, some air is recovered from the shear-layers in this region. In fact, the data seems to support the recovery concept. So, it is suggested that the vortex cores not need be adequate to support the entire shear layer, but perhaps just the high-velocity, most tightly entrained, portions. Then, the more slowly moving attached portion of the shear layer would be the air most susceptible to recovery. Although this is an appealing concept and fits the present data nicely, it is not yet sufficiently supported by data or observations.

Pressure Driven Air Entrainment

Referring to the modified form of the model of Campbell & Hilborne ($C_{Q,CHm}$ defined in Eq. 10), the velocity of air through the vortex tubes must be ascertained. As the true vortex tubes may certainly range in description from a cloud of bubbles to a clean air-filled tube-like structure, a single velocity is difficult to deduce. However, given the repeatable nature of these events in the physical record and knowing that it is needed for the model, it is suspected that a representative value can be found. Campbell and Hilborne [5] assumed a value equal to the free-stream velocity, and mentioned the uncertainty in this assumption. Rather than directly alter this approximation, consider it combined with separated shear layer effects. Define a pressure driven term as the difference between $C_{Q,CHm}$ and $C_{Q,Spurk}$ and use the recovery factor to determine when shear-effects are significant. This further modified rate is then

$$C_{Q,p} = \max\left(C_{Q,CHm} - C_{Q,Spurk}, 0\right)\left(1-\frac{k_{RQ}}{k_{RQ,Hys}}\right)^2 .$$

Within this context, $C_{Q,CHm}$ and $C_{Q,Spurk}$ both assume that $V_{VT}=V_\infty$. Therefore, they concurrently assume vortex-tube cross-sectional areas. Thus, this particular model assumes a vortex velocity behavior of

$$V_{VT} = V_\infty\left(1-\frac{k_{RQ}}{k_{RQ,Hys}}\right)^2 .$$

The combined results are plotted in Fig. 13 and conform nicely to the data.

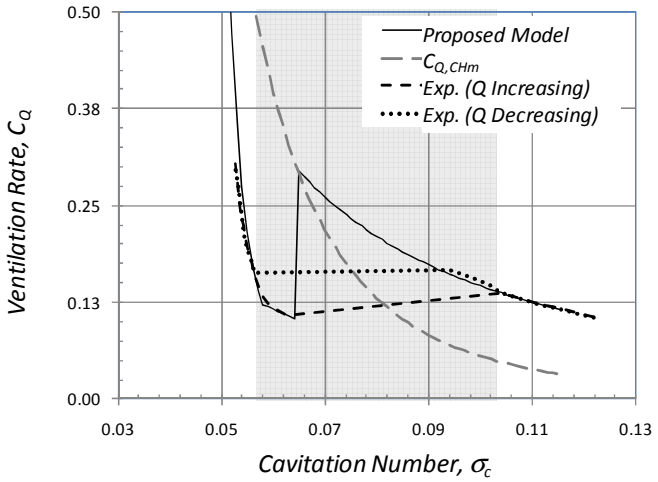

Figure 13: Air entrainment rates using the proposed model, Campbell & Hilborne model ($C_{Q,CHm}$), and experiments from Campbell and Hilborne [5].

Application of Model

Finally, the model is applied over a broad range of Froude numbers to display that it continues to produce valid results outside of this single case. Using the 1 inch diameter cavitator data from the experiments of Campbell and Hilborne [5], the model results show to continue to produce valid results in Fig. **14**. Note that the model predicts the entrainment rate quite reasonably though this range, and although not plotted,

similarly for the entire data set from Campbell and Hilborne [5]. In these cases, the empirical parameters (*A0, A2, and* $k_{RQ,Hys}$) are established using a least-squares fit to the data. Furthermore, the constant k_Q is determined using the observation from Fig. 12 that $C_{Q,CHm}$ and $C_{Q,Spurk}$ intersect at the lowest C_Q point that can sustain a twin-vortex cavity. Note that this is only observed for a single case and needs additional hysteretic data for further assessment. In any case, this allows the approximation of the toroidal-vortex cavity ventilation rates as well as the components from shear mechanisms.

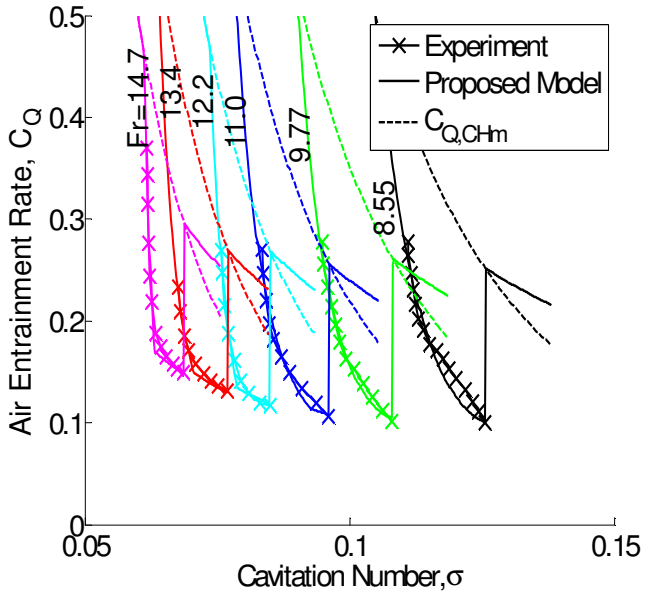

Figure 14: Air entrainment rates using the proposed model, Campbell & Hilborne model ($C_{Q,CHm}$), and experiments from Campbell and Hilborne [5].

Summary of the Present Model

As the model is developed throughout the preceding, it is summarized here. From Eq. 13 we define the air entrainment rate as the combination of shear-layer air and air exiting through pressure-gradient mechanisms as.

$$C_Q = C_{Q,SL} + C_{Q,p}\,. \tag{18}$$

The shear-layer air is defined through a modified form of the model of Spurk, accounting for separated via a recovery factor, given by Eq. 14 as

$$C_{Q,SL} = \left(1 - k_{RQ}\right) C_{Q,Spurk} \quad \&$$
$$C_{Q,Spurk} = k_Q \frac{\left(1+\sigma\right)}{\sigma}\sqrt{\frac{1}{\sigma}\ln\frac{1}{\sigma}}\,. \tag{19}$$

Note that recovery factor is presently an empirically determined term, estimated here using Eq. 15. Finally, the pressure driven term is given by the difference between the shear layer air and the equivalent vortex size. Then assuming a modified model for the axial velocity through the vortex tube. The model is given as

$$C_{Q,p} = \max\left(C_{Q,CHm} - C_{Q,Spurk}, 0\right)\left(1 - \frac{k_{RQ}}{k_{RQ,Hys}}\right)^2 \tag{20}$$
$$\& \quad C_{Q,CHm} = \frac{\pi A^2 \left(1+\sigma\right)^2}{47.6 k Fr_{N,Disk}^4 \sigma^4}\,.$$

These terms account for the proposed form of the model.

CONCLUSIONS

CFD has been used to analyze the air flow within supercavities. Results strongly corroborate the theory of Spurk [1] derived for toroidal cavities, suggesting this theory is relevant to cavities closing with twin-vortices and on bodies as well. For twin-vortex closing cavities, the theory of Spurk, requires modulation.

These CFD results were used to arrive at improved models of air entrainment, address issues with CFD turbulence modeling approaches, and highlight potential experimental scaling issues. When applied straightforwardly RANS approaches tend to over predict the amount of air entrained within cavity shear layers, ultimately overpredicting C_Q. Next, Reynolds number effects of the internal cavity air flow are evident. Although integral effects may be small, such as cavity size and/or pressure, the internal flow effect is significant. This may be an overlooked scaling issue. Lastly, an improved air-entrainment model is proposed that combines classical theory with that of Spurk [1] and accounts for the shear-layer air recovery.

Application of numerical simulations in this fashion is not a substitution for physical experiments. However, the computational modeling applied is expected, with sufficient resolution, to fully support the physical phenomena observed. Regardless of this, only physical experiments are expected to be able to validate or correct the conclusions drawn here.

Ventilated supercavities developed behind axisymmetric cavitators are known to follow scaling relationships that fix the dimensionless cavity size and cavity pressure given the ventilation rate and Froude number. For a largely steady cavity, it is also appropriate to treat the ventilation and an entrainment rate as an identity. The essence of the cavity air entrainment process is the cavity interface attached air shear layer. This was made clear by Spurk [1]. The entrainment process begins rather abruptly as the ventilation air feeds the shear layer. The shear layer develops from the cavitator detachment point to the cavity terminus. However, the air velocity profile is actually negative with respect to the moving interface. Therefore adverse pressure gradients, typically occurring at the aft end of the cavity, tend to stabilize, and thin the shear layer. As the entrained shear layer develops, the local amount of entrained air grows until the cavity reaches its maximum diameter. At the maximum diameter, the amount of shear layer entrained air is also a maximum but, as it is convected aftward, it is gradually diminished until the region of cavity closure. At the cavity closure region, the amount of air actually departing the cavity is finally determined. If the closure mechanism is toroidal vortex, the shear layer entrained air at the closure will exit unabated. If

the closure mechanism is twin vortex, some portion of the shear layer entrained air will be stripped off and recovered.

ACKNOWLEDGMENTS

This work was supported by the Office of Naval Research, under contract #N00014-07-1-0134, with Dr. Kam Ng as contract monitor. Furthermore, much gratitude is given to Dr. David Hill, Dr. Mark Maughmer, Dr. Phillip Morris, and Dr. Ralph Noack of The Pennsylvania State University for their comments and insights added with respect to this work.

NOMENCLATURE

Symbols

C_L	three-dimensional lift coefficient, $L/(q_\infty A)$
C_D	three-dimensional drag coefficient, $D/(q_\infty A)$
C_Q	ventilation rate coefficient, $QV_\infty^{-1}D^{-2}$
$C_{Q,l}$	local air entrainment rate, $\alpha u/V_\infty$
$C_{Q,CHm}$	modified Campbell and Hilborne model of C_Q
$C_{Q,Spurk}$	modified Spurk model of C_Q
$C_{Q,p}$	pressure-gradient driven C_Q terms
$C_{Q,SL}$	shear-layer driven C_Q terms
D_N	cavitator diameter
g	gravity
H	heavyside function
k_Q	empirical constant for shear-layer entrainment rate
k_{RQ}	portion of recovered shear-layer air
L_c	cavity length
Q	ventilation rate
R_c	cavity radius
R_N	cavitator radius
Re	Reynolds number, $\rho VL/\mu$
V	velocity
V_{VT}	axial velocity in vortex tube

Greek Symbols

α	air volume fraction
μ	molecular viscosity
ν	dynamic viscosity
ρ	density
σ_c	cavitation number based on cavity pressure, $(p_\infty - p_c)/q_\infty$

Subscripts

c	reference to cavity properties
Disk	reference shape to an effective disk
l	reference to local properties
N	reference to cavitator diameter
∞	reference to free stream

REFERENCES

[1] Spurk, J.H. "On the Gas Loss from Ventilated Supercavities," *Acta Mechanica*, vol. 155, pp. 125-135, 2002.

[2] May, A., "Water Entry and the Cavity-Running Behavior of Missiles," Naval Sea Systems Command Hydroballistics Advisory Committee Technical Report 75-2, 1975.

[3] Semenenko, V.N., "Artificial Supercavitation. Physics and Calculation," VKI Lecture Series on Supercavitating Flows, VKI Press, Brussels, Feb. 2001.

[4] Logvinovich, G.V., *Hydrodynamics of Free-Boundary Flows*, Israel Program for Scientific Translation, 1969.

[5] Campbell, I.J., Hilborne, D.V., "Air Entrainment Behind Artificially Inflated Cavities," 2nd Symposium on Naval Hydrodynamics, Washington D.C., USA, 1958.

[6] Lindau, J.W., Kunz, R.F., Boger, D.A., Stinebring, D.R., and H.J. Gibeling, "High Reynolds number, unsteady, multiphase CFD modeling of cavitating flows," *Journal of Fluids Engineering*, Transactions of ASME, vol. 124(3) pp. 607-616, 2002.

[7] Kinzel, M. P. Computational Techniques and Analysis of Cavitating-Fluid Flows. Dissertation in Aerospace Engineering, University Park, PA, USA : The Pennsylvania State University, May 2008.

[8] Kiceniuk, T., "An Experimental Study of the Hydrodynamic Forces Acting on a Family of Cavity Producing Conical Bodies of Revolution," California Institute of Technology-Hydrodynamics lab, Report E-12-17, June 1954.

[9] Wosnik, M., Schauer, T.J., and Arndt R.E.A., "Experimental Study of a Ventilated Supercavitating Vehicle," Fifth International Symposium on Cavitation (CAV2003), Osaka, Japan, November 1-4, 2003.

[10] Schauer, T.J., "An Experimental Study of a Ventilated Supercavitating Vehicle, MS Thesis, Department of Aerospace Engineering and Mechanics, University of Minnesota, 2003.

[11] •Kinzel, M.P., Lindau, J.W., Peltier, L.J., Zajaczkowski, F., Arndt, R.A., Wosnik, M., Mallison, T., "Computational Investigations of Air Entrainment, Hysteresis, and Loading for Large-Scale, Buoyant Cavities," 9th International Conference on Numerical Ship Hydrodynamics, Ann Arbor, Michigan, August 5-8, 2007.

[12] •Kinzel, M.P., Lindau, J.W., Peltier, L.J., Kunz, R.F, and Sankaran, V., "Detached-Eddy Simulations for Cavitating Flows," AIAA Paper No. 2007-4098, 18th AIAA Computational Fluid Dynamics Conference, Miami, FL, USA, June, 2007.

[13] ZHANG X.-w., WEI Y.-j., ZHANG J.-z., WANG C., YU K.-p., "Experimental research on the shape characters of natural and ventilated supercavitation," (2007) Journal of Hydrodynamics, 19 (5), pp. 564-571.